A ligand motif enables differential vascular targeting of endothelial junctions between brain and retina

Fenny H. F. Tang[a], Fernanda I. Staquicini[b,c], André A. R. Teixeira[a], Jussara S. Michaloski[a], Gislene M. Namiyama[d], Noemi N. Taniwaki[d], João C. Setubal[a], Aline M. da Silva[a], Richard L. Sidman[e,1], Renata Pasqualini[b,c], Wadih Arap[b,f], and Ricardo J. Giordano[a,1]

[a]Department of Biochemistry, Institute of Chemistry, University of São Paulo, São Paulo, SP 05508-000, Brazil; [b]Rutgers Cancer Institute of New Jersey, Newark, NJ 07103; [c]Division of Cancer Biology, Department of Radiation Oncology, Rutgers New Jersey Medical School, Newark, NJ 07103; [d]Electron Microscopy Laboratory, Institute Adolfo Lutz, São Paulo, SP 01246-000, Brazil; [e]Department of Neurology, Harvard Medical School, Boston, MA 02115; and [f]Division of Hematology/Oncology, Department of Medicine, Rutgers New Jersey Medical School, Newark, NJ 07103

Contributed by Richard L. Sidman, December 3, 2018 (sent for review June 4, 2018; reviewed by Matthew Campbell and Patricia A. D'Amore)

Endothelial heterogeneity has important implications in health and disease. Molecular markers selectively expressed in the vasculature of different organs and tissues are currently being explored in targeted therapies with promising results in preclinical and clinical studies. Noteworthy is the role that combinatorial approaches such as phage display have had in identifying such markers by using phage as nanoparticles and surrogates for billions of different peptides, screening noninvasively the vascular lumen for binding sites. Here, we show that a new peptide motif that emerged from such combinatorial screening of the vasculature binds selectively to blood vessels in the brain in vivo but not to vessels in other organs. Peptides containing a conserved motif in which amino acids Phenylalanine–Arginine–Tryptophan (FRW) predominate could be visualized by transmission electron microscopy bound to the junctions between endothelial cells in all areas of the brain, including the optic nerve, but not in other barrier-containing tissues, such as intestines and testis. Remarkably, peptides containing the motif do not bind to vessels in the retina, implying an important molecular difference between these two vascular barriers. Furthermore, the peptide allows for in vivo imaging, demonstrating that new tools for studying and imaging the brain are likely to emerge from this motif.

blood–brain barrier | blood–retina barrier | brain endothelial cells | peptide | phage display

Vascular endothelial heterogeneity has central implications in health and disease (1). Receptors selectively expressed in the vasculature of different organs and tissues are currently being explored in ligand-directed strategies for targeted imaging and therapy, with promising results in preclinical and clinical settings (2–5). Phage display has played an essential role in the identification of such receptors by screening noninvasively the vascular endothelium of different organ and tissues, in physiological and pathological conditions (i.e., tumor vessels) (6–8) (Fig. 1 *A* and *B*). The brain is a highly vascularized organ (9) shielded from most blood-borne molecules by a specialized blood–brain barrier (BBB) constituted by endothelial cells that are further enveloped by a layer of pericytes and astrocytes (9, 10). The BBB allows only the passage of gases, water, and small lipophilic molecules from blood into the brain parenchyma. Since brain endothelial cells are linked to one another by tight junctions, nutrients and waste products have to be shuttled across endothelial cell cytoplasm by a complex series of specialized transport systems (9–11). Remarkably helpful as this selectivity is for normal brain function, the BBB is a crucial obstacle for entry of therapeutic molecules in CNS diseases (8, 9, 12). Therefore, understanding molecular signatures unique to these barriers represents a key step toward development of novel treatment strategies (12). Several BBB markers have been identified in health and disease (13–16), all of which are ubiquitously expressed throughout the CNS. Nevertheless, the blood–retina barrier (BRB) and the blood–spinal barrier, commonly considered as part of the BBB (9, 11, 15, 17), have not been studied to the same extent and represent unique gateways for targeted development of regionally specific therapies for CNS disorders (18).

Results and Discussion

Here, we combined in vivo phage display technology with next-generation sequencing (NGS) to discover and exploit molecular signatures associated with the vasculature of the mouse brain (Fig. 1*A*). Phage display selection can be used to probe the vascular lumen of blood vessels in vivo, and to identify native ligand–receptor interactions that may be undetectable by tissue-destructive approaches such as genomics and proteomics. Thus, our screening strategy goes beyond molecular expression and takes into consideration tissue architecture and ligand–receptor accessibility (7). Our original screening here has been designed to select peptide sequences that target blood vessels serving different anatomical regions of the brain (Fig. 1*B*). A cyclic CX8C (X8, any eight residues; C, cysteine) phage library displaying $\sim 10^{10}$ unique sequences (19, 20) was administered i.v. into a single mouse (round I of selection), and, after 30 min of systemic circulation, phage particles bound to blood vessels in different brain regions (cerebellum, olfactory bulb, and hemispheres)

Significance

Endothelial barriers are essential components of blood vessels and particularly important in brain and retina, which are protected by barriers so efficient that almost all metabolites have to be actively transported across them. We provide evidence that short peptides containing a motif rich in amino acids with aromatic and positively charged side chains target specifically blood vessels of the brain but not of other tissues. Using electron microscopy, phage could be visualized bound to the endothelial junction of these vessels, demonstrating how these two techniques can be combined to identify a supramolecular phage target in vivo. Surprisingly, this peptide motif does not bind to vessels in the retina, implying a previously unknown molecular difference between these endothelial junctions.

Author contributions: F.H.F.T. and R.J.G. designed research; A.A.R.T., J.S.M., G.M.N., and N.N.T. performed research; F.I.S., J.C.S., A.M.d.S., and R.P. contributed new reagents/analytic tools; R.L.S., R.P., W.A., and R.J.G. analyzed data; and R.L.S., R.P., W.A., and R.J.G. wrote the paper.

Reviewers: M.C., Trinity College Dublin; and P.A.D., Schepens Eye Research Institute of Massachusetts Eye & Ear.

The authors declare no conflict of interest.

[1]To whom correspondence may be addressed. Email: richard_sidman@hms.harvard.edu or giordano@iq.usp.br.

This article contains supporting information online at www.pnas.org/lookup/suppl/doi:10.1073/pnas.1809483116/-/DCSupplemental.

Published online January 22, 2019.

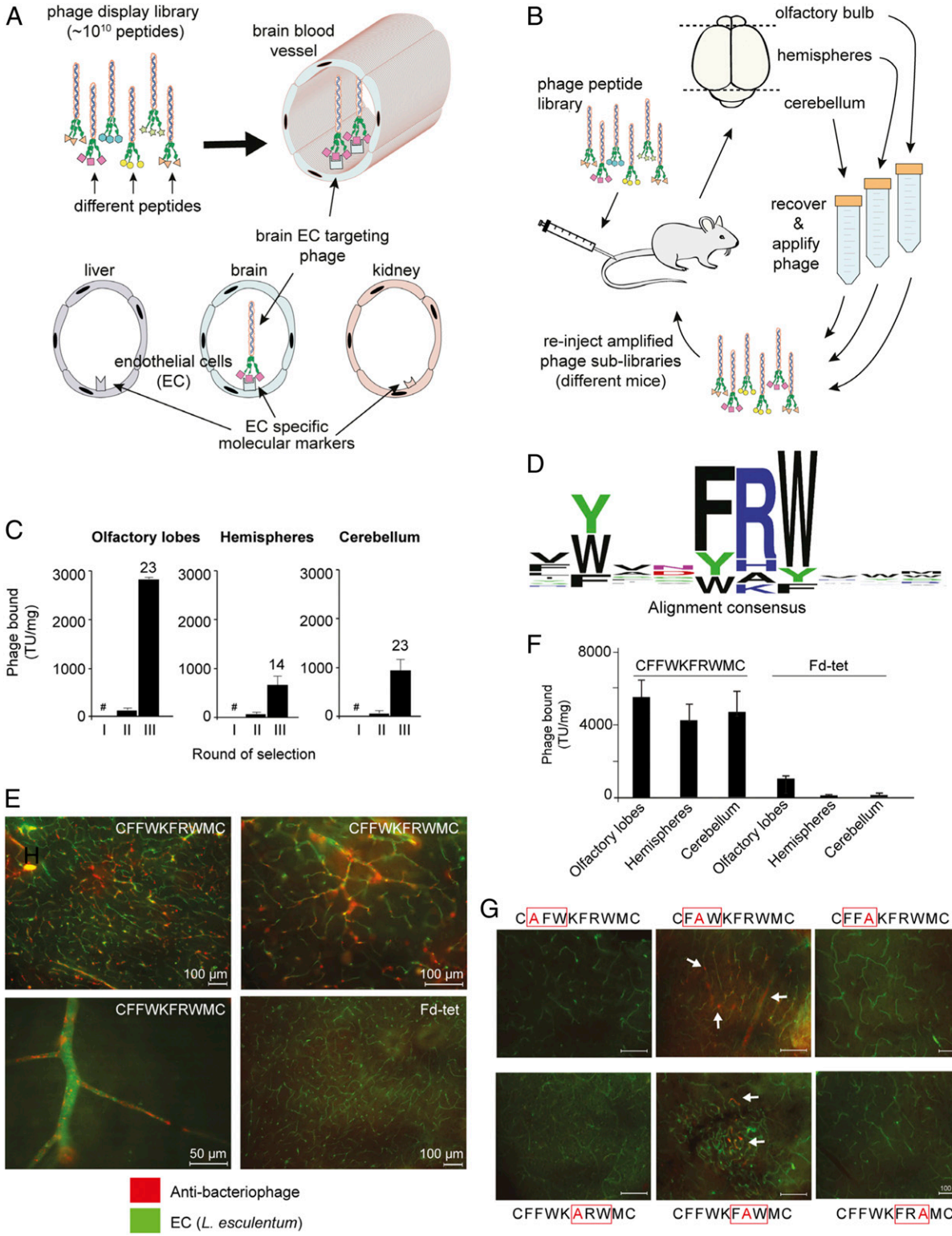

Fig. 1. Identification of a peptide motif that targets brain blood vessels. (*A*) Phage display library selection identifies peptides targeting blood vessels. In the CX8C phage library, the ligand peptides are fused to minor capsid protein III (pIII) assembled at one end of the virion. (*B*) Phage display in vivo scheme. (*C*) Number of phage particles (TU normalized per milligram of tissue) recovered in each round of selection per brain region. The number above each bar indicates phage enrichment in round III relative to round II; #, round I was not quantified, to minimize loss of unique peptides. (*D*) Alignment of the total pool of unique peptides (n = 1,021) reveals the consensus motif FRW. (*E*) Phage CFFWKFRWMC or negative control Fd-tet phage (10^9 TU) were administered i.v. into mice, and phage bound to blood vessels in brain hemispheres is visualized with antibacteriophage sera (red) and blood vessels with FITC-conjugated *Lycopersicon* (Tomato) *esculentum* lectin (green). (Scale bars: 100 μm, unless otherwise indicated.) (*F*) Quantification by colony count of phage bound to different regions of the mouse brain (n = 4). (*G*) Effect on phage homing caused by different Ala mutations within the FRW motif. Bars represent means ± SEM from triplicates. (Scale bars: 100 μm.)

were recovered and amplified separately. Following the first round of selection, each phage pool was then readministered i.v. in successive mice for the next round of selection. After three rounds of i.v. selection, we observed marked phage enrichment in all brain regions, including 23-fold to the olfactory bulb, 14-fold to the brain hemispheres, and 23-fold to the cerebellum from selection rounds II to III (Fig. 1*C*). Initial analysis by Sanger DNA sequencing revealed that several selected DNA sequences encoding targeting peptides to different brain regions contained a prevalent ligand motif rich in aromatic amino acid residues [Phenylalanine (Phe) and Tryptophan (Trp)] along with a recurrent positively charged residue in between them (*SI Appendix*, Fig. S1). This finding was unexpected, considering that the subsequent rounds II and III of selection were performed independently, and yet a unique dominant motif has emerged from the individual screenings, a result indicative of ligand selection. Next, NGS of all phage-displayed peptides (21) recovered in each round of selection identified 1,021 distinct targeted peptides sharing the pattern [FYW]-X-X-[FYW][ARKH][FYW] (Fig. 1*D*) (*SI Appendix*, *Supplementary Data Alignment File*).

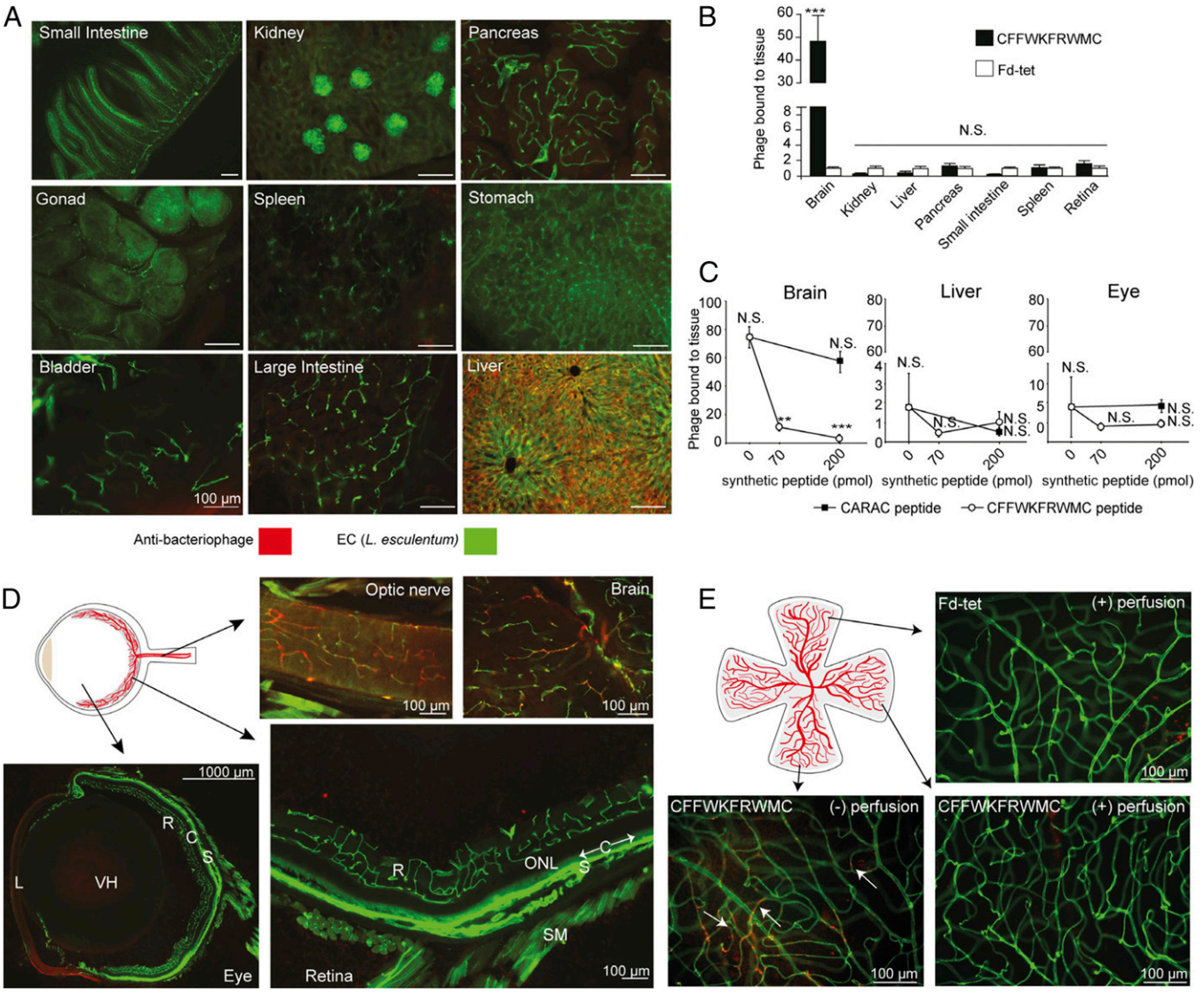

Fig. 2. CFFWKFRWMC peptide is specific for intracranial brain vasculature but not retinal vessels. (*A*) Targeted CFFWKFRWMC-displaying phage bound to blood vessels in different tissues visualized by immunofluorescence with antibacteriophage antisera (red) and FITC-conjugated *L. esculentum* lectin (green). (Scale bars: 100 μm.) (*B*) Quantification by colony count of phage bound to blood vessels in different tissues. To account for variability due to differences in tissue vascular areas, phage binding (in transducing units per milligram) was normalized relative to the control phage (Fd-tet). Bars represent means ± SEM from two independent experiments (each with $n = 2$ animals, and $n = 4$ retinas) and triplicate plating for colony count. Statistical test used two-way ANOVA. N.S., not significant; $^{***}P \leq 0.001$. (*C*) Peptide competition assay. Animals were injected with synthetic peptides (CFFWKFRWMC or a control peptide) before phage administration. Phage homing (in transducing units per milligram) was normalized relative to the control phage (Fd-tet). Bars represent means ± SEM from quadruplicate plating for colony count ($n = 1$ animal per condition, with $n = 2$ retinas or brain and liver halves). Statistical test used one-way ANOVA. $^{***}P \leq 0.0005$. (*D*) Immunofluorescence detection of phage CFFWKFRWMC bound to the optic nerve and brain, while the eye's retinal and choroidal blood vessels are negative. Vascular layers of the inner retina (R) and nonvascular (therefore invisible) outer nuclear layer (ONL) are shown. The monolayered nonvascular (and also invisible and unlabeled) retinal pigment epithelium lies immediately internal to the choroid (*C*), which is indicated with arrows along segments of its length. The sclera (S), lens (L), smooth muscle (SM), and vitreous humor (VH) are also indicated. (Scale bars: 100 μm, except where noted.) (*E*) Immunofluorescence detection of phage in retina whole mounts from mice injected with phage CFFWKFRWMC or Fd-tet under two different conditions: perfused (+) or not perfused (–) with fixative solution to remove unbound circulating phage. Arrows indicate positive phage staining. (Scale bars: 100 μm.)

Of note is the presence of aromatic amino acids flanking a positively charged residue, of which 432 (42%) of unique ligand peptides contained a tripeptide Phe–Arginine–Trp (Phe-Arg-Trp) (herein denominated as the FRW motif).

Index phage particles displaying CFFWKFRWMC were selected as a representative of the FRW motif class because it was one of the most abundant ligand peptides identified (*SI Appendix*, Table S1). Either targeted CFFWKFRWMC-displaying phage or control phage (insertless Fd-tet) was administered i.v. into mice, and phage bound to the vasculature was visualized by immunofluorescence and quantified by bacterial infection and transducing unit (bacterial colony) count. We observed that CFFWKFRWMC-displaying phage particles bind to endothelial cell surfaces of small and larger blood vessels in all areas examined within the brain (Fig. 1 *E* and *F*), whereas no binding to the vasculature above background was observed with the control phage. Interestingly, we observed an uneven staining of the vasculature with a consistent "spotty" pattern, and, while most if not all vessels were positive for phage staining, some vessels displayed a more robust staining than others (Fig. 1*E*, high-magnification image). Targeting seemed dependent on the FRW motif, since site-directed mutagenesis with alanine (Ala) scanning markedly abrogated phage binding in vivo. One should note that our chosen index peptide may perhaps contain two putatively targeting motifs (displayed sequence CFFWKFRWMC, underline indicates the two motifs), although the first one lacks a positively charged residue. In-tandem assays consisting of site-directed ligand motif mutagenesis plus i.v. targeting in vivo with CFFWKFRWMC revealed that either Phe to Ala or Trp to Ala completely abolished brain homing, while mutations in the middle residues of both motifs diminished but did not entirely abolish binding to brain blood vessels (Fig. 1*G*, arrows, and *SI Appendix*, Fig. S2). These results suggest that the first and third motif positions carrying amino acid residues with aromatic side chains are essential for binding, while the second position (often occupied by the positively charged residues) is more permissive. Interestingly, although, among the selected peptides, only 62 unique peptides out of 1,021 (6.1%) (*SI Appendix*, *Supplementary Data Alignment File*) contained an Ala in between the two hydrophobic residues (FAW), one of them (CLYVNFAWRC) was among the most abundant isolated in the biopanning along with phage CFFWKFRWMC (*SI Appendix*, Table S1). Together, these results suggest that presence of a positively charged residue either between the aromatic residues or adjacent to the motif is important for high-affinity binding.

To determine whether binding of phage CFFWKFRWMC is specific to brain blood vessels, we analyzed its presence in other tissues. No phage was detected by immunofluorescence in small intestine, kidney, pancreas, gonads, spleen, stomach, bladder and large intestine (Fig. 2*A*), results that were again confirmed by colony counting (Fig. 2*B*). Both targeted and control insertless phage nonspecifically accumulated at similarly high levels in the liver, suggesting no preferential binding of either phage to the hepatic vasculature (Fig. 2*B* and *SI Appendix*, Fig. S3), an observation entirely consistent with the collective previous experience with reticuloendothelial system (RES)-rich control organs such as liver and spleen (6). To further confirm our observations and that targeting to blood vessels was mediated by the peptide, we performed a competition experiment. Animals were first inoculated i.v. with synthetic peptide CFFWKFRWMC (70 and 200 pmol) or a control peptide before phage administration. We observed that the preadministration of the cognate synthetic peptide inhibited phage homing to brain only, but not to other tissues (Fig. 2C and *SI Appendix*, Fig. S4). The control peptide had no significant effect. Phage homing to liver was not affected by the synthetic peptide, again suggesting no specific targeting of the hepatic vasculature.

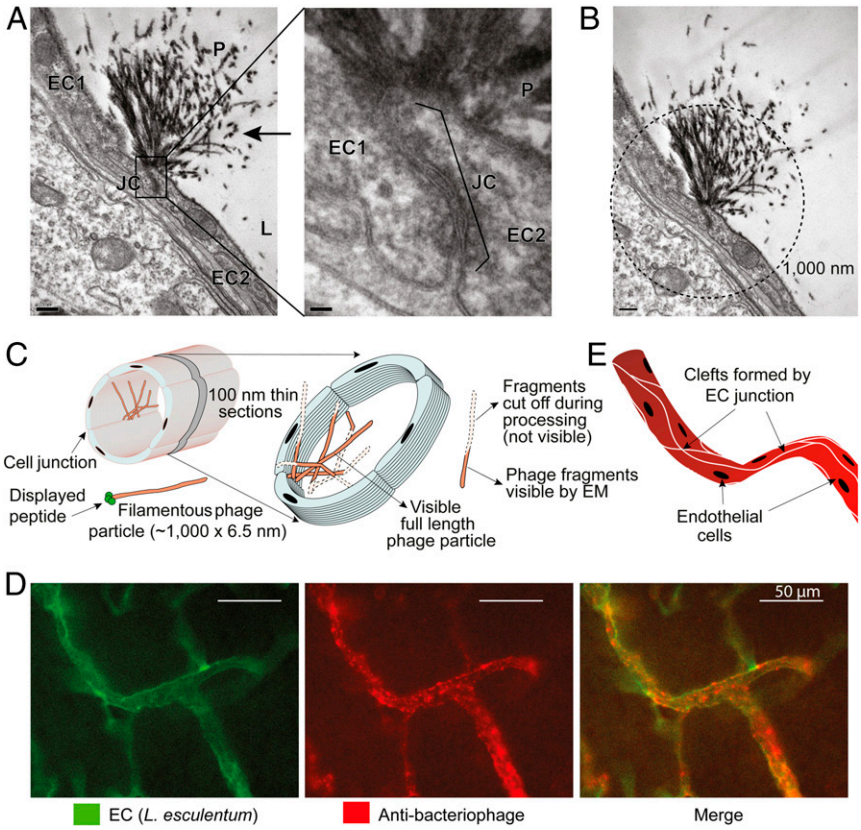

Fig. 3. CFFWKFRWMC peptide targets brain endothelial junctions. (*A*) TEM images of brain from a mouse receiving i.v. targeted CFFWKFRWMC-displaying phage (10^{10} TU) (100-nm section). *Left* (magnification 10,000×) shows lumen (L) and junction (JC) of two endothelial cells (EC1 and EC2). The typical morphology of filamentous phage (P) is indicated (arrow). *Right* depicts a higher magnification (60,000×) highlighting the junction between two endothelial cells. (Scale bars: 200 nm.) (*B*) Calculated length of the phage tufts. Circle in dashed lines indicates 1,000-nm diameter centered at the base of the endothelial junction. (Scale bar: 20 nm.) (*C*) Schematic illustration of the observed phage tufts in 100-nm thin sections. (*D*) Immunofluorescence detection of targeted CFFWKFRWMC-displaying phage bound to cell clefts formed by junctions and branches of endothelial cells of blood vessels in the brain. (*E*) Schematic illustration of the clefts of endothelial cells formed along the longitudinal axis of the blood vessels.

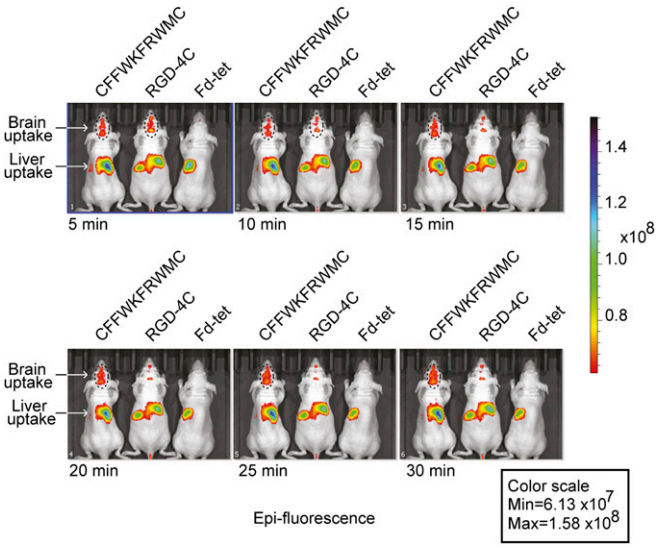

Fig. 4. CFFWKFRWMC peptide as a tool for imaging in vivo. NIR imaging of mice given a single i.v. dose of targeted CFFWKFRWMC-displaying phage, negative control Fd-tet, or αv integrin-binding RGD-4C-phage conjugated to NIR dye IRDye 680RD. Images were acquired in different time courses and show NIR fluorescence accumulation in the liver (nonspecific RES trapping) and brain areas. Epifluorescence color scale calibration bar for the images is on the right.

The fact that the cognate synthetic peptide inhibits phage homing to the brain indicates it might be possible to develop improved synthetic peptidomimetic versions for theranostic purposes. Peptidomimetic versions of CFFWKFRWMC should not be taken up the liver and would allow for better assessment of its possible interaction with liver vasculature. Together, these results confirm that binding of phage CFFWKFRWMC is mediated by the peptide and is specific to brain blood vessels.

However, we have also observed that phage CFFWKFRWMC does not bind to retinal blood vessels, an intriguing result confirmed by both colony count and immunostaining (Fig. 2 *B*–*E*). In contrast, targeted phage binding was also detected in blood vessels of the optic nerve (Fig. 2*D*), which carry blood immediately preceding the optic nerve vessel branches that enter the retina. Further experiments with whole retinas also confirmed this observation. Moreover, when the experiment was repeated and animals were not perfused to remove unbound circulating phage, we detected phage particles in the retina, confirming that phage CFFWKFRWMC reaches the retina but does not accumulate in this tissue (Fig. 2*E*). Since these studies were initially performed in the albino BALB/c mouse strain, we asked whether retinal mutations specific to this mouse strain could be responsible for the blood vessel differences between retina and the rest of the brain. We therefore repeated the experiments with the visually competent C57BL/6J mouse strain, with similar results. The lack of interaction of CFFWKFRWMC-displaying phage particles with blood vessels in the retina are, therefore, unlikely to be due to inherited genetic mutations carried by these animals or physiological deficiencies in the retina, and are likely caused by molecular differences between these CNS vascular territories. This is a striking result considering that the blood–retina barrier is believed to have very similar properties to the BBB (10, 11). To our knowledge, this is potentially a previously unknown BBB molecular target that is not present in the blood vessels of the retina; moreover, the ligand FRW motif may differentially target BBB from the BRB.

To gain insight into receptor expression and location, we have next performed transmission electron microscopy (TEM) studies. M13-derived phage particles can be easily identified by their long filamentous morphology (22). Indeed, in mice receiving CFFWKFRWMC-displaying phage, we observed tufts formed by long thin electron-dense filaments bound to and accumulated at the junctions between endothelial cells in the brain (Fig. 3*A*). These tufts have the expected morphology and ∼1,000-nm size of phage particles (Fig. 3*B*), and were unlike any other cellular structure found in mouse brain or other tissues. These filaments were bound to the cell junction by one end of the phage, in agreement with fusion of peptide CFFWKFRWMC to the pIII coat proteins located at one end of the virion filament (Figs. 1*A* and 3*C*). The tuft pattern also indicates that multiple phage particles are bound to and accumulated at the endothelial cell junctions (Fig. 3*C*), explaining the strong dotted signal observed by epifluorescence microscopy. These TEM results are, therefore, in agreement with the immunofluorescence staining pattern in which phage seems to accumulate in a spotted pattern, often next to blood vessel junctions or branches (Fig. 3*D*). Indeed, phage binding seems to follow the intercellular clefts formed by the endothelial cells elongated and joined to one another along the axis of the blood vessels (Fig. 3*E*) (23). The endothelial cells form a layer closest to the lumen in blood vessels, and, in the brain, are well known to have very tight intercellular junctions. It is likely that CFFWKFRWMC binds to proteins or other molecules associated with these cell–cell tight junctions (11). Whether peptide CFFWKFRWMC binds directly to molecules present at the endothelial junctions or to cell surface receptors, which then move along the membrane for endocytosis, resulting in formation of phage tufts at the cell junctions, will need to be addressed by further studies.

Finally, real-time visualization in vivo is essential for understanding normal biological processes as well as for the development of novel diagnostic methods for human diseases. To show that the FRW motif can be used to image the brain in vivo, phage were labeled with a near-infrared (NIR) fluorescent dye and administered i.v. into BALB/c nude mice (24). Strong brain epifluorescence was detected in mice treated with NIR dye-labeled phage CFFWKFRWMC or RGD-4C (sequence CDCRGDCFC, an αv integrin-binding double-cyclic motif) (Fig. 4). No epifluorescence was observed with the NIR dye-labeled negative control phage (Fd-tet) and with phage CFFWKFRWMC in the retina (ex vivo) (*SI Appendix*, Fig. S5). Most importantly, phage carrying the FRW motif accumulated longer in the mouse brain, resulting in strong epifluorescent signals that lasted for more than 30 min, compared with phage particles displaying the RGD-4C targeting peptide.

In summary, we have selected and identified a ligand peptide motif that targets endothelial cell junctions present in blood vessels of the brain part of the CNS, but not the retina, suggesting a molecular difference between the BBB and the BRB, two important blood–CNS barriers. Targeted small peptidomimetics containing an FRW motif may serve as a theranostic developmental drug lead for translational applications for CNS diseases.

Methods

Animals. All experiments were reviewed and approved by the Institutional Animal Care and Utilization Committees of the Chemistry Institute of the University of São Paulo and the University of New Mexico Health Science Center. We used female BALB/c and C57BL/6J mice (The Jackson Laboratory) maintained at the animal facility of the Institute of Chemistry and Pharmacy School of the University of São Paulo and female immunodeficient BALB/c athymic mice (Charles River Laboratory) maintained at the animal facility of the University of New Mexico Health Science Center. Animals were kept on a 12-h light/dark cycle. Rodent chow and water were available ad libitum.

Phage Library Construction. The cyclic phage display (CX8C) library used in the study was built as previously described (20). For details, see *SI Appendix, SI Materials and Methods*.

Synthetic Peptides. Peptides were synthesized and purified by HPLC to a purity greater than 95% by Chinese Peptide Company. Two peptides were used in this study: peptide CFFWKFRWMC and peptide CARAC (referred to as control) (25).

Identification of Brain-Targeting Peptides by Phage Display in Vivo. To isolate peptides targeting the brain, animals received the CX8C phage library [10^9 transducing units (TU)] by i.v. injection. After 30 min in circulation, mice were perfused with 20 mL of DMEM, and phage bound to tissue were recovered by tissue homogenization followed by bacterial infection, amplified, and used for two more rounds of selection. After the final round, random bacterial colonies were selected for DNA sequencing to identify phage coding peptides targeting each brain area. For details, see *SI Appendix, SI Materials and Methods*.

Phage Sequencing. Sanger sequencing was performed at the sequencing facility at the Institute of Chemistry, University of São Paulo, as previously described (20, 25). High-throughput DNA sequencing was performed using the MiSeq Reagent Kit v2 (500 cycles) on an Illumina MiSeq equipment at the Center for Advanced Technologies in Genomics at Institute of Chemistry, University of São Paulo. For details, see *SI Appendix, SI Materials and Methods*.

Validation of Phage Homing in Vivo. Phage homing in vivo to different tissues and organs was performed by colony count and immunofluorescence as described (2). In brief, phage was injected i.v. into mice, and, after 30 min of circulation, animals were perfused through the heart, and phage bound to blood vessels was detected by immunofluorescence using bacteriophage antisera or quantified by bacterial infection followed by colony counting. For details, see *SI Appendix, SI Materials and Methods*.

Site-Directed Mutagenesis of CFFWKFRWMC Phage Particles. Mutant phage particles displaying alanine-scanning variants of CFFWKFRWMC were prepared by site-directed PCR mutagenesis as described (2). For details, see *SI Appendix, SI Materials and Methods*.

TEM. Animals were injected i.v. with 10^{10} TU of CFFWKFRWMC phage or control Fd-tet phage. After 30 min, they were perfused through the heart with fixative solution (2.5% glutaraldehyde:4% paraformaldehyde in 0.1 M phosphate monobasic/dibasic buffer, pH 7.4). Brain tissues were postfixed with 1% (wt/vol) osmium tetroxide (OsO_4), and 0.5% uranyl acetate was used as contrast. Ultrathin sections (100 nm) were stained with uranyl acetate and lead citrate and observed with a transmission electron microscope (model JEM1011; JEOL) operating at 80 kV. For details, see *SI Appendix, SI Materials and Methods*.

Imaging in Vivo with CFFWKFRWMC Phage. Phage particles were labeled with IRDye 800CW and used for imaging in vivo as described (24). NIR fluorescent images were acquired serially over 5- to 30-min time periods and analyzed using the IVIS Spectrum In Vivo Imaging System (PerkinElmer). For ex vivo fluorescence quantification, retina, brain, and liver were dissected and analyzed with an Odyssey Infrared Imaging Scanner. For details, see *SI Appendix, SI Materials and Methods , refs. 1–8*.

Statistics. All numerical data are expressed as mean ± SEM. We analyzed data sets for significance, with one-way ANOVA or two-way ANOVA (Prism GraphPad software). *P* values of less than 0.05 were considered to be statistically significant.

Data Availability. The authors declare that all data supporting the findings in this study are available within the article and *SI Appendix* or from the corresponding author on reasonable request.

ACKNOWLEDGMENTS. We thank Maria L. Baldini and Celia Ludio A. Braga for technical assistance. This study was supported by Research Grants 2009/54.806-8 and 2014/21.177-9 (to R.J.G.) from São Paulo Research Foundation and by the National Council for Scientific and Technological Development (CNPq). F.H.F.T. was supported by a fellowship from the Coordination for the Improvement of Higher Education Personnel (CAPES) - Finance Code 001. A.M.d.S., J.C.S., and R.J.G. received Research Fellowship Awards from CNPq. The funders had no role in study design, data collection, analysis, decision to publish, or preparation of the manuscript.

1. Aird WC (2012) Endothelial cell heterogeneity. *Cold Spring Harb Perspect Med* 2: a006429.
2. Giordano RJ, et al. (2008) Targeted induction of lung endothelial cell apoptosis causes emphysema-like changes in the mouse. *J Biol Chem* 283:29447–29460.
3. Barnhart KF, et al. (2011) A peptidomimetic targeting white fat causes weight loss and improved insulin resistance in obese monkeys. *Sci Transl Med* 3:108ra112.
4. Lorusso D, et al. (2012) Phase II study of NGR-hTNF in combination with doxorubicin in relapsed ovarian cancer patients. *Br J Cancer* 107:37–42.
5. Pasqualini R, et al. (2015) Targeting the interleukin-11 receptor α in metastatic prostate cancer: A first-in-man study. *Cancer* 121:2411–2421.
6. Arap W, et al. (2002) Steps toward mapping the human vasculature by phage display. *Nat Med* 8:121–127.
7. Ozawa MG, et al. (2008) Beyond receptor expression levels: The relevance of target accessibility in ligand-directed pharmacodelivery systems. *Trends Cardiovasc Med* 18: 126–132.
8. Staquicini FI, et al. (2011) Systemic combinatorial peptide selection yields a non-canonical iron-mimicry mechanism for targeting tumors in a mouse model of human glioblastoma. *J Clin Invest* 121:161–173.
9. Tam SJ, Watts RJ (2010) Connecting vascular and nervous system development: Angiogenesis and the blood-brain barrier. *Annu Rev Neurosci* 33:379–408.
10. Park-Windhol C, D'Amore PA (2016) Disorders of vascular permeability. *Annu Rev Pathol* 11:251–281.
11. Díaz-Coránguez M, Ramos C, Antonetti DA (2017) The inner blood-retinal barrier: Cellular basis and development. *Vision Res* 139:123–137.
12. Bicker J, Alves G, Fortuna A, Falcão A (2014) Blood-brain barrier models and their relevance for a successful development of CNS drug delivery systems: A review. *Eur J Pharm Biopharm* 87:409–432.
13. Obermeier B, Daneman R, Ransohoff RM (2013) Development, maintenance and disruption of the blood-brain barrier. *Nat Med* 19:1584–1596.
14. Obermeier B, Verma A, Ransohoff RM (2016) The blood-brain barrier. *Handb Clin Neurol* 133:39–59.
15. Wilhelm I, Nyúl-Tóth Á, Suciu M, Hermenean A, Krizbai IA (2016) Heterogeneity of the blood-brain barrier. *Tissue Barriers* 4:e1143544.
16. Librizzi L, et al. (2018) Cerebrovascular heterogeneity and neuronal excitability. *Neurosci Lett* 667:75–83.
17. Campbell M, Humphries P (2012) The blood-retina barrier: Tight junctions and barrier modulation. *Adv Exp Med Biol* 763:70–84.
18. Marchiò S, Sidman RL, Arap W, Pasqualini R (2016) Brain endothelial cell-targeted gene therapy of neurovascular disorders. *EMBO Mol Med* 8:592–594.
19. Beppler J, et al. (2016) Negative regulation of bacterial killing and inflammation by two novel CD16 ligands. *Eur J Immunol* 46:1926–1935.
20. Michaloski JS, Redondo AR, Magalhães LS, Cambui CC, Giordano RJ (2016) Discovery of pan-VEGF inhibitory peptides directed to the extracellular ligand-binding domains of the VEGF receptors. *Sci Adv* 2:e1600611.
21. Dias-Neto E, et al. (2009) Next-generation phage display: Integrating and comparing available molecular tools to enable cost-effective high-throughput analysis. *PLoS One* 4:e8338.
22. Souza GR, et al. (2006) Networks of gold nanoparticles and bacteriophage as biological sensors and cell-targeting agents. *Proc Natl Acad Sci USA* 103:1215–1220.
23. Adamson RH (1993) Microvascular endothelial cell shape and size in situ. *Microvasc Res* 46:77–88.
24. Dobroff AS, et al. (2016) Towards a transcriptome-based theranostic platform for unfavorable breast cancer phenotypes. *Proc Natl Acad Sci USA* 113:12780–12785.
25. Giordano RJ, Cardó-Vila M, Lahdenranta J, Pasqualini R, Arap W (2001) Biopanning and rapid analysis of selective interactive ligands. *Nat Med* 7:1249–1253.